Progress In Electromagnetics Research, PIER 71, 59–83, 2007

EFFECT OF CYLINDRICAL SCATTERER WITH ARBITRARY CURVATURE ON THE FEATURES OF A METAMATERIAL SLAB ANTENNA

C. A. Valagiannopoulos

School of Electrical and Computer Engineering
National Technical University of Athens
GR 157–73, Zografou, Athens, Greece

Abstract—The metamaterial slab with low refractive index exhibits directive properties which make it suitable to work as antenna. The characteristics of such a device are affected under the presence of a conducting rod of arbitrary shape placed over the slab. A qualitative and quantitative approach is presented which is possible by implementing the method of auxiliary sources. For the evaluation of the far field quantities the method of stationary phase is employed. A validation example considering a circular rod is solved rigorously with use of the method of moments. Several numerical results are shown and discussed.

1. INTRODUCTION

During the last years an increasing amount of attention has been attracted by artificial materials synthesized by inserting suitable periodic structures in usual host media, which are known as metamaterials. This surge of interest reflects the numerous practical applications in which metamaterials can be employed. In [1] transmission lines constructed by metamaterial structures (with negative refractive index) are used for the design of a compact, broadband balun for two wire antennas, while in [2] a compact resonator which is partially occupied by a metamaterial ring is analyzed and proven to have interesting properties. Metamaterials can also reduce drastically the total scattering cross section of electrically large objects in case they are used as coatings [3].

Metamaterial slabs in particular, have been the subject of many publications examining waveguiding and radiation properties of these structures. For example in [4] a metamaterial grounded slab is

investigated. The supported propagation constants are extracted and the waveguiding conditions lead to the suppression of a guided–wave regime for both polarizations. Similar analyses are presented in [5–7] where surface and guided waves are observed and examined. Moreover in [7] slabs of metamaterials are studied by solving the related electric–type integral equation via the method of moments.

One basic application of a metamaterial slab is the directive property demonstrated when its refraction index is close to zero. The idea applies Snell's law [8] for rays inside a low index metamaterial (LIM). Because of the small refractive index the transmission angle is forced to have values close to zero. Therefore the exiting ray from the substrate will be normal to the surface. This property can be used to control the direction of emission and thus is extensively exploited in designing radiation devices. In [9] an antenna with LIM substrate is proposed while in [10–13] there are several analyses concerning similar structures and certain numerical results indicating their good radiation characteristics.

Such high directivity devices are useful for both signal transmission and object detection. In the present paper, the effect of an arbitrary obstacle placed in the near field of these antennas is examined. Suppose that a small (and almost invisible) object is located close to the radiation emitter. It will probably negatively influence the device's properties by "blinding" the radar operation or "jamming" the emitted directive field and in this sense such a study can have military applications. But apart from negative effects we think that a qualitative and quantitative description may be useful even for improving the radiation features of the device in certain cases. An investigation for similar purposes but concerning a different directive emission is presented in [14].

We specifically regard a perfect electric conducting (PEC) rod of arbitrary shape placed over a LIM substrate backed by a PEC plane. The structure is excited by a source placed inside the LIM substrate. We first determine the Green's function of this configuration and the incident field in the absence of the scatterer; this is achieved with the use of spectral integrals and enforcement of the necessary boundary conditions.

In view of the arbitrary shape of the rod an analytical approach is not possible and a numerical procedure is utilized instead. We implement the method of auxiliary sources (MAS) for estimating the scattering field by the cylinder. In this process the computed Green's function is necessary. As we refer to an antenna the basic quantity we are interested about is the far field and this is derived by estimating asymptotically the spectral integrals through the method of stationary

phase.

In order to verify the results of the numerical method, we solve analytically the problem in the special case of a circular cylindrical PEC scatterer. The surface current on this is expressed in modal form as a sum of harmonics and computed by solving the related integral equation rigorously. Several analytic formulas with Bessel functions are used.

A satisfactory coincidence between the results of the two methods and a very low error in the boundary condition are observed (for circular cross section). For the general case the error is kept below a small upper limit for all the applications. After assuring the validity of the proposed method we study features such as the surface current, the maximum radiation power, the 3 db beamwidth, the radiation pattern and the relative radiation power. The variations of the above quantities are depicted as functions of the azimuthal angle, the shape and the size of the scatterer, the thickness of the substrate and the position of the excitation source.

2. PROBLEM FORMULATION

The configuration of the problem is shown in Fig. 1. Both the cartesian (x, y, z) and cylindrical (ρ, ϕ, z) coordinate system are used interchangeably. A time dependence of the form $e^{j\omega t}$ is suppressed. Consider a slab of finite thickness $D-d$ constructed by a homogeneous LIM backed by a ground plane and posed inside vacuum. In this example the medium can be characterized by a plasma frequency close to the operating one $\omega = 2\pi f$. Its intrinsic parameters are denoted by $(\epsilon_1\epsilon_0, \mu_1\mu_0)$ where (ϵ_0, μ_0) are the ones of the vacuum and $0 < \epsilon_1, \mu_1 \ll 1$. For the local wavenumbers and impedances are used the symbols $k_1 = k_0\sqrt{\epsilon_1\mu_1}, \zeta_1 = \zeta_0\sqrt{\frac{\mu_1}{\epsilon_1}}$ (for LIM area 1) and k_0, ζ_0 (for vacuum area 0).

The excitation is an infinite filamentary electric current of constant magnitude I Amperes located across the axis $(x = 0, y = -t)$ with $0 < d < t < D$, that is into the metamaterial slab which occupies the region between planes $y = -d, -D$. Due to Snell's law all the exiting rays from the slab will be close to normal to the surface. Therefore not only directivity but also control of the emission direction is achieved. The emitted field is scattered by a PEC infinite (in the z direction) cylinder with arbitrary shape. The origin of the coordinate system is located inside the cylinder. The outer surface of the scatterer is defined by an arbitrary polar function $\rho = R(\phi) > 0$. As the configuration of the device is invariant across z axis and so is the excitation, it is natural for the response of the system to own the same property. Hence all

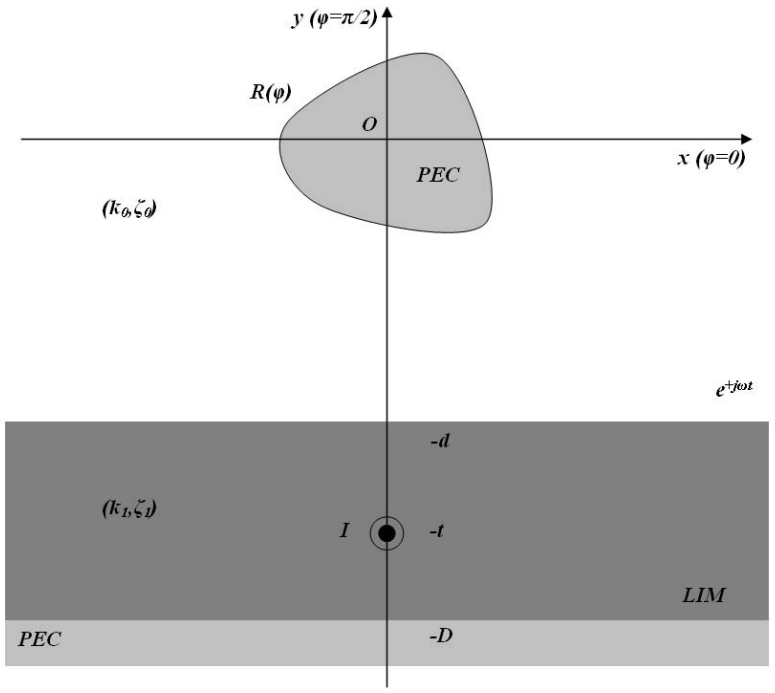

Figure 1. The physical configuration of the investigated structure. The slab of low index metamaterial (LIM) is backed by a perfectly electric conducting (PEC) plane and excited by current I. The produced field is scattered by the PEC cylinder of arbitrary shape.

the field quantities are independent of z (functions of x, y or ρ, ϕ only). Furthermore, due to the source which is an electric current, the only nonzero field components will be E_z (single axial electric component) and (H_x, H_y) or alternatively (H_ρ, H_ϕ) [16].

The purpose of the present analysis is to estimate the effect of the PEC scatterer (rod) to the radiation pattern of the antenna in the far field.

3. GREEN'S FUNCTION AND INCIDENT FIELD

The aims of this section are two: the derivation of the electric type Green's function of the problem and the determination of the incident field developed due to the excitation source inside the slab antenna. Both quantities are computed in the absence of the cylindrical

scatterer. The Green's function of electric type is a solution of the two–dimensional problem concerning the axial electric field produced by a filamentary electric current with magnitude $j/(k\zeta)$ in Amperes (with the adopted time dependence) [16]. The wavenumber and the impedance of the area into which the Green's source lies are denoted by k and ζ respectively. The axis of the filament is referred with capitals: $(x = X, y = Y)$ or $(\rho = P, \phi = \Phi)$ instead. As the arbitrary rod is placed into area 0, the same should be true for the Green's source, that is $Y > -d$. It is well–known [17] that the free–space Green's function is given by

$$G_{0,singular}(x, y, X, Y) = -\frac{j}{4} H_0^{(2)}\left(k_0\sqrt{(x-X)^2 + (y-Y)^2}\right) \quad (1)$$

where $H_0^{(2)}$ is the cylindrical Hankel function of zeroth order and second type. The same function can be written as a spectral integral

$$G_{0,singular}(x, y, X, Y) = \frac{1}{4\pi}\int_{-\infty}^{+\infty} \frac{e^{-\mu_0(\beta)|y-Y|}}{\mu_0(\beta)} e^{-j\beta(x-X)} d\beta \quad (2)$$

where $\mu_0(\beta) = \sqrt{\beta^2 - k_0^2}$ is the so–called radiation function of area 0. Note that the integration path on complex β plane is the real axis.

As opposed to the singular free–space function, the quantity expressing the reaction of the area 0 will be smooth. A similar integral representation is utilized corresponding to the solution of the homogeneous Helmholtz equation in a semi–infinite area.

$$G_{0,smooth}(x, y, X, Y) = \frac{1}{4\pi}\int_{-\infty}^{+\infty} C_0(\beta) \frac{e^{-\mu_0(\beta)(y+d)}}{\mu_0(\beta)} e^{-j\beta(x-X)} d\beta \quad (3)$$

In order for the y–dependent component to fulfill Sommerfeld's radiation condition, both parts of $\mu_0(\beta)$ should be positive (or zero): $\Re[\mu_0(\beta)], \Im[\mu_0(\beta)] \geq 0$. As far as the area 1's expression is concerned, the two y–dependent components cancel so that the total quantity is vanishing at $y = -D$ (PEC plane).

$$G_1(x, y, X, Y) = \frac{1}{4\pi}\int_{-\infty}^{+\infty} C_1(\beta) \frac{\sinh(\mu_1(\beta)(y+D))}{\mu_1(\beta)} e^{-j\beta(x-X)} d\beta \quad (4)$$

where $\mu_1(\beta) = \sqrt{\beta^2 - k_1^2}$ is the radiation function of area 1 and $C_0(\beta), C_1(\beta)$ determinable functions not only of the integration variable β but of the Green's source position (X, Y) as well.

After the enforcement of the proper boundary conditions at $y = -d$, one reaches the explicit formula of $G_{0,smooth}$ in cylindrical coordinates:

$$G_{0,smooth}(\rho,\phi,P,\Phi) = \int_{-\infty}^{+\infty} C_G(\beta)\, e^{-\rho(j\beta\cos\phi+\mu_0(\beta)\sin\phi)} e^{-P(-j\beta\cos\Phi+\mu_0(\beta)\sin\Phi)} d\beta \quad (5)$$

where:

$$C_G(\beta) = \frac{1}{4\pi}\frac{e^{-2d\mu_0(\beta)}}{\mu_0(\beta)}\frac{k_1\zeta_1\mu_0(\beta) - k_0\zeta_0\coth((D-d)\mu_1(\beta))\mu_1(\beta)}{k_1\zeta_1\mu_0(\beta) + k_0\zeta_0\coth((D-d)\mu_1(\beta))\mu_1(\beta)} \quad (6)$$

The total Green's function for area 0 is denoted without the second subscript

$$G_0(\rho,\phi,P,\Phi) = G_{0,singular}(\rho,\phi,P,\Phi) + G_{0,smooth}(\rho,\phi,P,\Phi) \quad (7)$$

For the derivation of the incident electric field a similar procedure will be followed. Now the singular component belongs to area 1 ($x = 0, y = -t$) and thus the corresponding reaction quantity does not by itself ensure the demand for vanishing electric field at $y = -D$. After trivial algebraic manipulations the incident electric field into area 0 is found to be

$$E_{0,inc}(\rho,\phi) = \int_{-\infty}^{+\infty} C_E(\beta)\, e^{-\rho(j\beta\cos\phi+\mu_0(\beta)\sin\phi)} d\beta \quad (8)$$

where

$$C_E(\beta) = \frac{Ik_0\zeta_0k_1\zeta_1}{2\pi j} e^{-\mu_0(\beta)d} \cdot \frac{\sinh((D-t)\mu_1(\beta))}{k_0\zeta_0\cosh((D-d)\mu_1(\beta))\mu_1(\beta) + k_1\zeta_1\sinh((D-d)\mu_1(\beta))\mu_0(\beta)} \quad (9)$$

As area 0 is semi–infinite the integrand functions of the fields in all regions to possess the branch points of the function $\mu_0(\beta)$, namely $\beta = \pm k_0$ [18]. The same functions are even with respect to $\mu_1(\beta)$, a property indicating the finite thickness of area 1. In the integral representation of $G_{0,smooth}$, the branch points are also singular, constituting integrable poles.

4. AUXILIARY SOURCES AND FAR FIELD

The method of auxiliary sources (MAS) is a numerical technique suitable for a variety of scattering problems. It is based on the

principle of imposing the boundary conditions only on a finite number of discrete points of the physical boundaries [19], called collocation points. The fields in each area satisfy the Helmhotz equation as they are weighted sums of the local Green's functions corresponding to singular elementary sources (auxiliary sources) posed on a set of points. It should be stressed that for the estimation of the field in a region, it is supposed that the remaining area is filled with the same material with the investigated one. The auxiliary sources are placed outside the region whose field they represent so that the inner field is smooth, as a result of scattering. The same procedure is repeated for each region of the problem. Sometimes it is convenient to group adjacent regions and to employ the modified Green's functions which incorporate the additional boundary conditions [20].

In the investigated problem we regard the entire configuration in the absence of the scatterer as one region and the scatterer itself as another (that is why we computed G_0 in the previous section). Given the fact that the cylinder is perfectly conducting we simply have to find the field in the surrounding region. This can be approximately produced by a finite distribution of discrete electric filamentary currents in the interior region of the rod (after this has been temporarily removed). The surface on which the auxiliary sources are posed, is called the auxiliary surface and usually is similar to the boundary [21]. In our case the bound is defined through $\rho = R(\phi)$ and therefore the auxiliary surface is chosen to have the polar equation $\rho = sR(\phi)$ with $0 < s < 1$. When it comes to the distribution of the auxiliary sources, the most common choice is to place them on equispaced points [22]. Such a recipe can be followed in our case of arbitrary shape under the condition that function $R(\phi)$ is not rapidly varying with respect to ϕ. Otherwise more sources should be located near regions with abrupt variation of curvature. We choose N equispaced points $(sR(\Phi_n), \Phi_n)$ for $n = 0, ..., N-1$. This implies that the length of the curve between each adjacent auxiliary sources should be equal to the total length of the line (auxiliary surface in two dimensions) divided by N. If one supposes $\Phi_0 = 0$ the other auxiliary polar angles Φ_n are found via the following equation [23]

$$\int_{\Phi_n}^{\Phi_{n+1}} \sqrt{R^2(\phi) + R'^2(\phi)}d\phi = \frac{1}{N}\int_0^{2\pi} \sqrt{R^2(\phi) + R'^2(\phi)}d\phi \qquad (10)$$

where $R'(\phi)$ is the derivative of $R(\phi)$ with respect to ϕ.

The scattered electric field is

$$E_{0,scat}(\rho, \phi) = \sum_{n=0}^{N-1} A_n G_0(\rho, \phi, sR(\Phi_n), \Phi_n) \qquad (11)$$

where A_n are unknown complex constants expressed in V/m. The boundary condition of the vanishing tangential electric field upon the PEC surface $E_{0,inc}(R(\phi),\phi)+E_{0,scat}(R(\phi),\phi)=0$ will be imposed for N discrete collocation points. These are chosen to be the points of the scatterer's outer surface located at the same polar angles Φ_m). In this way the following linear $N\times N$ system is formulated (from which A_n are determined):

$$\sum_{n=0}^{N-1} A_n G_0\left(R\left(\Phi_m\right),\Phi_m,sR\left(\Phi_n\right),\Phi_n\right)=-E_{0,inc}\left(R\left(\Phi_m\right),\Phi_m\right) \quad (12)$$

The issue of choosing s, in other words "how close to the outer surface should the auxiliary one be placed?" has attracted attention [24] as it is significant for the proper implementation of the method. In our case where auxiliary sources and collocation points are located on the same azimuthal angles Φ_n, the condition number of the system's matrix gets lower as s gets close to unity with fixed N. That is because for $s\to 1$ the matrix is close to diagonal (always $s<1$ because for $s=1$ the Green's function is singular). On the other hand for fixed s the condition number of the matrix is increasing with N (size of the matrix). We thus use a high enough N in order to obtain convergent results (satisfying the boundary condition) with an s suitably close to 1 so that the matrix of the system is numerically invertible.

As it stated above we are mainly interested in the effect of the arbitrary cylinder in the radiation pattern of the slab antenna. For this reason we need to compute the Green's functions and incident field as $\rho\to+\infty$ for $0<\phi<\pi$. Both $E_{0,inc}$ and $G_{0,smooth}$ are of the form

$$w\left(\rho,\phi\right)=\int_{-\infty}^{+\infty} W\left(\beta\right)e^{-\rho(j\beta\cos\phi+\mu_0(\beta)\sin\phi)}d\beta \quad (13)$$

In the investigated region $\sin\phi>0$ and it is also imposed that $\Re[\mu_0(\beta)]\geq 0$. Therefore in the limit $\rho\to+\infty$ the integration interval should be restricted to $(-k_0,k_0)$. Now the phase of the exponential term is purely real (as the integration path is also real) and defined by

$$p\left(\beta\right)=\beta\cos\phi+\sqrt{k_0^2-\beta^2}\sin\phi \quad (14)$$

For $0<\phi<\pi$ the only stationary point of the phase is $\beta=k_0\cos\phi$. By applying the stationary phase technique [25], one arrives at the asymptotic expansion:

$$w\left(\rho,\phi\right)\sim\pi k_0\sin\phi W\left(k_0\cos\phi\right)\sqrt{\frac{2}{\pi k_0\rho}}e^{-jk_0\rho+j\frac{\pi}{4}},\rho\to+\infty \quad (15)$$

From (8) and (13) with use of (15), the far field expression of $E_{0,inc}$ is

$$E_{0,inc}(\rho,\phi) \sim \pi k_0 \sin\phi C_E(k_0\cos\phi)\sqrt{\frac{2}{\pi k_0\rho}}e^{-jk_0\rho+j\frac{\pi}{4}}, \rho\to+\infty \quad (16)$$

The asymptotic formula for the free–space Green's function at large radial distances is well–known [26]

$$G_{0,singular}(\rho,\phi,P,\Phi) \sim -\frac{j}{4}e^{jk_0P\cos(\phi-\Phi)}\sqrt{\frac{2}{\pi k_0\rho}}e^{-jk_0\rho+j\frac{\pi}{4}}, \rho\to+\infty \quad (17)$$

By combining (17) and (15) for $G_{0,smooth}$ and substituting into (7) the total Green's function is evaluated in the far field.

$$G_0(\rho,\phi,P,\Phi) \sim \sqrt{\frac{2}{\pi k_0\rho}}e^{-jk_0\rho+j\frac{\pi}{4}}$$
$$\cdot\left(\pi k_0\sin\phi C_G(k_0\cos\phi)e^{jk_0P\cos(\phi+\Phi)} - \frac{j}{4}e^{jk_0P\cos(\phi-\Phi)}\right), \rho\to+\infty \quad (18)$$

From (11) through (18), one readily finds the asymptotic expansion of the scattered electric field $E_{0,scat}$.

5. VALIDATION EXAMPLE

The solution presented above is not a rigorous one and that is why it is necessary to compare the results with those derived by a more accurate method for a simpler case. In this section we determine the surface current upon the infinite cylindrical scatterer for the special case that its cross section is circular with radius $R(\phi) = a$. The procedure, for the most part, is fairly analytic. If one denotes the electric axial current upon PEC surface by $K(\phi)$ then the scattered field is written as [16]:

$$E_{0,scat}(\rho,\phi) = -jk_0\zeta_0 a\int_0^{2\pi} K(\Phi)\,G_0(\rho,\phi,a,\Phi)\,d\Phi \quad (19)$$

This integral equation for the surface current can be solved by expressing $K(\phi)$ as a Fourier sum $K(\phi) = \sum_{u=-\infty}^{+\infty} F_u e^{ju\phi}$ (modal solution). Imposing the boundary condition at $\rho = a$, multiplying by $e^{-jv\phi}$ for each integer v and integrating over $(0, 2\pi)$, yields

$$\sum_{u=-\infty}^{+\infty} F_u\int_0^{2\pi}\int_0^{2\pi} G_0(a,\phi,a,\Phi)\,e^{j(u\Phi-v\phi)}d\Phi d\phi =$$
$$-\frac{j}{k_0\zeta_0 a}\int_0^{2\pi} E_{0,inc}(a,\phi)\,e^{-jv\phi}d\phi \quad (20)$$

If one uses the well-known relation for Hankel function originating from addition theorem [27]

$$G_{0,singular}\left(\rho,\phi,P,\Phi\right)= \\ -\frac{j}{4}\sum_{r=-\infty}^{+\infty}H_r^{(2)}\left(k_0\max\left(\rho,P\right)\right)J_r\left(k_0\min\left(\rho,P\right)\right)e^{jr(\Phi-\phi)} \quad (21)$$

the sum of double integrals involving $G_{0,singular}$ is promptly evaluated.

$$\sum_{u=-\infty}^{+\infty}F_u\int_0^{2\pi}\int_0^{2\pi}G_{0,singular}\left(a,\phi,a,\Phi\right)e^{j(u\Phi-v\phi)}d\Phi d\phi= \\ -\frac{j}{4}\left(2\pi\right)^2J_v\left(k_0a\right)H_v^{(2)}\left(k_0a\right)F_v \quad (22)$$

With J_r we denote the Bessel function of order r.

As far as operations involving $G_{0,smooth}$ and $E_{0,inc}$ are concerned, the components dependent on ϕ or Φ are separated and expressed in exponential form. Those quantities can be integrated analytically through the formula

$$\int_0^{2\pi}e^{-g(\pm j\beta\cos c+\mu_0(\beta)\sin c)}e^{\mp jhc}dc=2\pi j^{\mp h}\left(\frac{\beta+\mu_0\left(\beta\right)}{k_0}\right)^{-h}J_h\left(k_0g\right) \quad (23)$$

where h is integer. This expression is derived with the change of variable $k_0\sin q=j\mu_0\left(\beta\right)$ and $k_0\cos q=\beta$. Also the logarithmic expressions of inverse harmonic functions [28] are utilized and the well–known integral representation of Bessel functions [17] is employed. If (23) is used twice, one obtains

$$\int_0^{2\pi}\int_0^{2\pi}G_{0,smooth}\left(a,\phi,a,\Phi\right)e^{j(u\Phi-v\phi)}d\Phi d\phi= \\ \left(2\pi\right)^2j^{u-v}k_0^{u+v}J_u\left(k_0a\right)J_v\left(k_0a\right)\int_{-\infty}^{+\infty}C_G\left(\beta\right)\left(\beta+\mu_0\left(\beta\right)\right)^{-u-v}d\beta \quad (24)$$

$$\int_0^{2\pi}E_{0,inc}\left(a,\phi\right)e^{-jv\phi}d\phi= \\ 2\pi j^{-v}k_0^vJ_v\left(k_0a\right)\int_{-\infty}^{+\infty}C_E\left(\beta\right)\left(\beta+\mu_0\left(\beta\right)\right)^{-v}d\beta \quad (25)$$

The linear system (with unknowns the complex F_u Fourier coefficients) is then truncated so that: $u,v=-U,...,U$. It is noticeable that after

the substitution of (22), (24) and (25) into (20) the function $J_v(k_0a)$ is factored. The $(2U+1)\times(2U+1)$ system is given by:

$$-\frac{j}{4}2\pi H_v^{(2)}(k_0a)F_v + 2\pi k_0^{u+v}\sum_{u=-U}^{U}F_u j^{u-v}J_u(k_0a)\int_{-\infty}^{+\infty}C_G(\beta)(\beta+\mu_0(\beta))^{-u-v}d\beta = -\frac{j}{k_0\zeta_0 a}j^{-v}k_0^v\int_{-\infty}^{+\infty}C_E(\beta)(\beta+\mu_0(\beta))^{-v}d\beta \quad (26)$$

As stated in [29], matrices of this form as the above guarantee numerical stability even for quite high U. For this reason the value of U will be determined exclusively by the convergence of the solution (unlike N which was dependent on other considerations as well).

The asymptotic expression of the scattered field for $\rho\to+\infty$ is deduced through (18) and (19):

$$E_{0,scat}(\rho,\phi)\sim -2\pi j k_0 a\zeta_0\sqrt{\frac{2}{\pi k_0\rho}}e^{-jk_0\rho+j\frac{\pi}{4}}\cdot \sum_{u=-U}^{U}F_uJ_u(k_0a)\,j^u\left(\pi k_0\sin\phi C_G(k_0\cos\phi)\,e^{-ju\phi}-\frac{j}{4}e^{ju\phi}\right),\ \rho\to+\infty \quad (27)$$

For the derivation of (27), (23) for $\beta=k_0$ was used twice.

6. NUMERICAL RESULTS

A set of programs has been developed to evaluate effectively the values of the scattered and incident electric field and compute their asymptotic expressions in the far region. The implementation of formulas such as (5), (8) and (26) requires the numerical computation of integrals whose functions possess branch points and poles. In particular, the expressions are dependent on the double valued quantity $\mu_0(\beta)=\sqrt{\beta^2-k_0^2}$ in such a way that its branch points and the shape of its branch cuts carry over to the aforementioned expressions. It is well–known that $\mu_0(\beta)$ has a real part of constant sign (positive or negative) for all complex β only when its branch cuts are chosen suitably. When $k_0>0$ the proper shape of branch cuts is shown in Fig. 2. These orthogonal lines are limiting forms of hyperbolas [30]. It is convenient to suppose that $\mu_0(\beta)$ possesses a positive real part. Moreover, the integrals with smooth functions at $\beta=\pm k_0$ are computed by numerical integration across the real axis with slight

vertical shifts to remain on the same Riemann sheet. The functions with integrable singularities will be integrated by bypassing $\beta = \pm k_0$ (otherwise the numerical procedures will be ruined) through a well–shaped path which is depicted in Fig. 2. The integral is, of course, independent of the wells' depths which were varied as a check. Also the integrals are of infinite integration path and therefore it should be truncated. This is feasible as all the integrands are decaying exponentially.

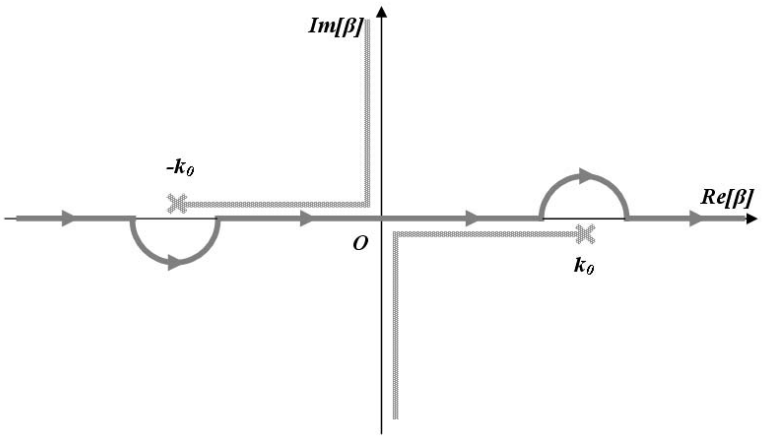

Figure 2. The proposed integration path for the numerical computations of the spectral integrals. The integrand function can exhibit integrable singularities at the branch points $\beta = \pm k_0$ (marked by X). Its branch cuts are the same with the radiation function's $\mu_0(\beta)$. The integral is independent of the radii of semi-circular circumventions.

Before proceeding to the numerical applications, certain checks assuring the validity of the proposed method should be made. In Fig. 3a we consider a circular rod and both presented methods are used for the computation of the scattering electric field across the boundary of the cylinder. The percent difference between the results of the two methods is presented. We assume a radius of $a = 1.5\,\text{cm}$ and a substrate having a thickness of $D - d = 4\,\text{cm}$ ($D = 8\,\text{cm}$ and $d = 4\,\text{cm}$) with the source posed in the middle $t = 6$ cm inside a material with relative parameters $\epsilon_1 = 0.01$ and $\mu_1 = 0.01$. Three operating frequencies are examined $f = 8, 10$ and $12\,\text{GHz}$. We also chose a unitary excitation current for simplicity $I = 1\,\text{A}$. Only half the azimuthal extent is studied $-\pi/2 < \phi < \pi/2$ owing to the symmetry of the configuration. We notice that the method of auxiliary sources is in good agreement with the rigorous modal solution of the integral

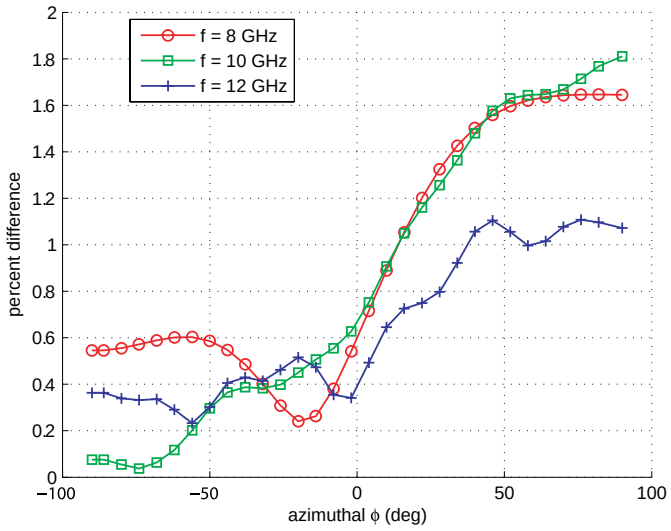

(a)

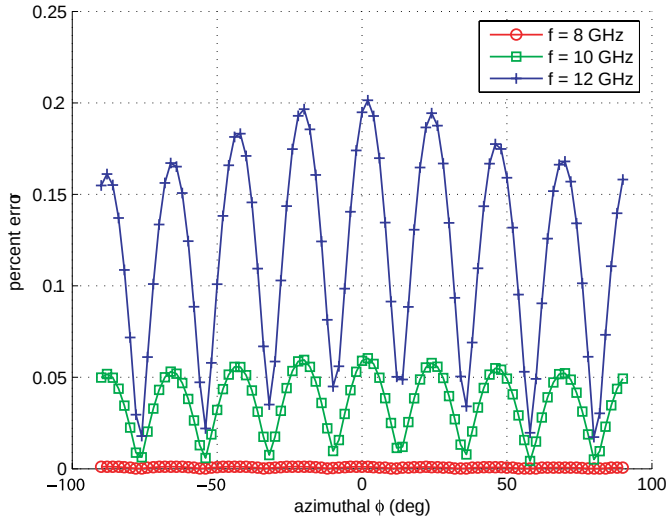

(b)

Figure 3. Validation quantities as function of azimuthal angle for various operating frequencies f. Only the variation for $-\pi/2 < \phi < \pi/2$ is presented due to symmetry. The rod is circular with radius $a = 1.5\,\text{cm}$. Other parameters: $\epsilon_1 = 0.01$, $\mu_1 = 0.01$, $I = 1\,\text{A}$, $D = 8\,\text{cm}$, $d = 4\,\text{cm}$, $t = 6\,\text{cm}$. (a) Percent difference of the scattered electric field on the surface computed by both methods. (b) Percent error of the boundary condition computed by rigorous method.

equation as the difference remains in all cases below 2%. The quantity in average is greater for $0 < \phi < \pi/2$. As a rule of thumb $N = 100$ auxiliary sources per wavelength of scatterer's radius are sufficient for a convergent result and a tolerable difference equal or less than the above. It should be combined with a choice of s close to unity such as $s = 0.93 - 0.97$. In Fig. 3b the percent error of the boundary condition with use of modal method is shown for the same configuration parameters. This method is very accurate as the maximum error does not exceed 0.2%. We remark that with increasing operating frequency the error becomes greater. That is because the same number of modes U is used, while the scatterer gets electrically larger. For excellent results $U = 15$ azimuthal harmonics per wavelength of scatterer's radius are adequate. In applications with non circular cross sections, convergence checks with respect to all the truncation parameters are made and a final confirmation of the boundary condition is performed with a maximum permissible error of 1%.

In order to examine the characteristics of the device under the presence of non circular scatterers, we regard an ellipse centered at the origin with semi major axis $a = 2\,\text{cm}$ and semi minor axis $b = 1\,\text{cm}$. The ellipse is rotated by angle δ with respect to x axis (with δ=0 the ellipse's major axis is parallel to the antenna plane). It can be shown that the polar equation of such a curve is given by

$$R(\phi) = \frac{ab}{\sqrt{(b\cos(\phi-\delta))^2 + (a\sin(\phi-\delta))^2}} \tag{28}$$

In Fig. 4a the radiated power $\lim_{\rho\to+\infty}\left[\rho|E_{0,scat}(\rho,\phi)+E_{0,inc}(\rho,\phi)|^2/\zeta_0\right]$ (in W/m) in the far field over the upper half plane is presented as function of the azimuthal angle $0 < \phi < \pi$. The operating frequency is taken equal to $f = 10\,\text{GHz}$, the other parameters are the same with the previous example and five cases of rotation angles are considered ($\delta = 0, \pi/6, \pi/4, \pi/3, \pi/2$). In all the investigated examples the maximum radiated power is exhibited at $\phi = \pi/2$. The magnitude of the radiated power at $\phi = \pi/2$ is higher for $\delta = \pi/4$ while for $\delta = 0, \pi/2$ and for $\delta = \pi/6, \pi/3$ the maximal quantity is similar. One could also point out that the sidelobes are stronger in the second quadrant ($\pi/2 < \phi < \pi$) than in the first one. In Fig. 4b the relative radiation quantity $\lim_{\rho\to+\infty}\left[|E_{0,scat}(\rho,\phi)+E_{0,inc}(\rho,\phi)|^2/|E_{0,inc}(\rho,\phi)|^2\right]$ (in db) is presented for the same parameters. This quantity normalizes the far field of the antenna to the far field in the absence of the scatterer in order to express the effect of the rod to the operation of the device. It should be stressed that almost for all the azimuthal angles the value

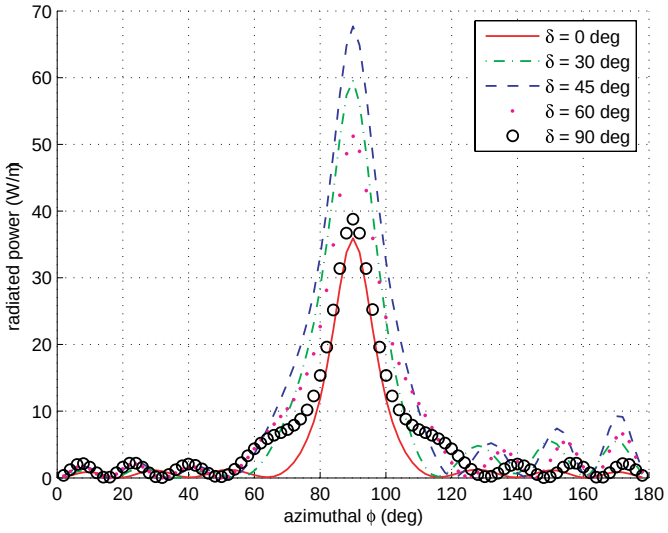

(a)

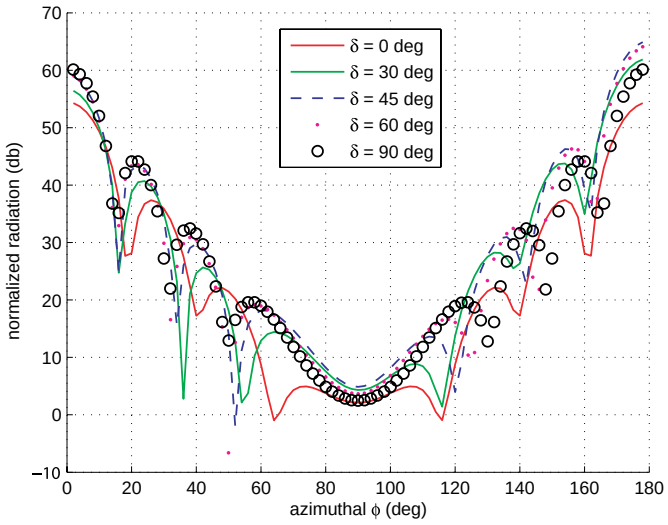

(b)

Figure 4. Variation of far field radiation quantities as function of the azimuthal ϕ for various rotation angles δ of the elliptical scatterer with semi axes $a = 2\,\text{cm}$ and $b = 1\,\text{cm}$. Other parameters: $\epsilon_1 = 0.01$, $\mu_1 = 0.01$, $I = 1\,\text{A}$, $f = 10\,\text{GHz}$, $D = 8\,\text{cm}$, $d = 4\,\text{cm}$, $t = 6\,\text{cm}$. (a) Radiated power (W/m) (b) Radiated power normalized by the corresponding power in the absence of the rod (db).

is positive indicating that the rod is converted to a secondary antenna which amplifies the radiation field of the initial structure for almost any direction. This is not beneficial for the antenna designer because the directivity is decreasing as the relative radiation quantity is much greater far from the maximum angle than in the vicinity of it ($\phi \cong \pi/2$). One can additionally point out that the graphs for $\delta = 0, \pi/2$ are symmetrical with respect to y axis. This is due to the symmetry and does not hold for general values of δ.

As mentioned above, the angle of maximum radiated power remains invariant in every numerical example ($\phi = \pi/2$) and therefore a noteworthy quantity will be the magnitude of maximum power (in W/m) as function of the rotation angle of the ellipse δ. In Fig. 5a we consider five different operating frequencies ($f = 8, 9, 10, 11, 12\,\mathrm{GHz}$). One can observe that the curves corresponding to $f = 8$ and $11\,\mathrm{GHz}$ are decreasing contrary to the one of $f = 9\,\mathrm{GHz}$ which is increasing. The other two curves possess a maximum in the middle of the interval. In the case of $f = 9\,\mathrm{GHz}$ little variation of the power is noticed, while a very large maximum appears at $\delta = 0$ for $f = 8\,\mathrm{GHz}$ approaching $200\,\mathrm{W/m}$. In Fig. 5b the 3 db beamwidth variance is presented with respect to the same parameters. The differences between the curves are initially (for $\delta = 0$) quite large and as δ increases the antenna's pattern has a 3 db extent between 15 and 20 degrees for all the regarded frequencies. Despite the presence of the scatterer which scrambles the radiation signal, the beamwidth for $f = 9\,\mathrm{GHz}$ remains remarkably low at 11.5 degrees for $\delta = 0$. Another point to be noted is that both maximum power and 3 db angle has similar variations with respect to δ.

The effect of the rod's shape on the characteristics of the device is worth examining. We consider an ellipse with constant semi minor axis $b = 1.5$ cm (normal to the antenna plane) and variable eccentricity ϵ. The polar function representing such a curve is given by:

$$R(\phi) = \frac{b}{\sqrt{(1-\epsilon^2)\cos^2\phi + \sin^2\phi}} \tag{29}$$

The operating frequency is taken equal to $f = 10\,\mathrm{GHz}$. In Fig. 6a we present the radiated power as function of azimuthal angle for various eccentricities ($\epsilon = 0, 0.5, 0.7, 0.8, 0.85$). An obvious conclusion is that the maximum power (at $\phi = \pi/2$) is increasing as ϵ increases. To put it alternatively larger surfaces develop higher currents and thus substantial fields are produced. The sidelobes have relatively low magnitudes and also are symmetrical with respect to y axis as the ellipse is not rotated. In Fig. 6b the normalized radiation quantity is presented with respect to the same variables. For constant ϕ this

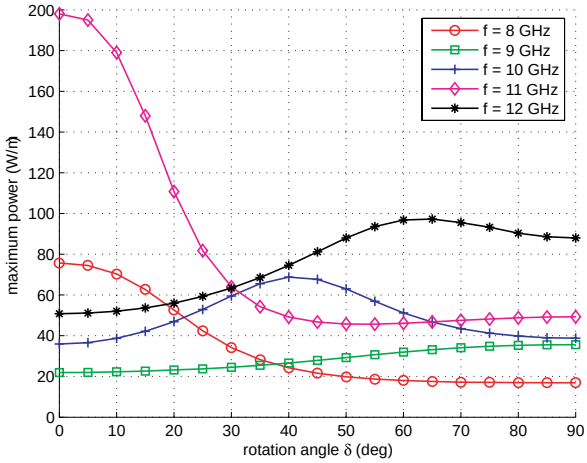

(a)

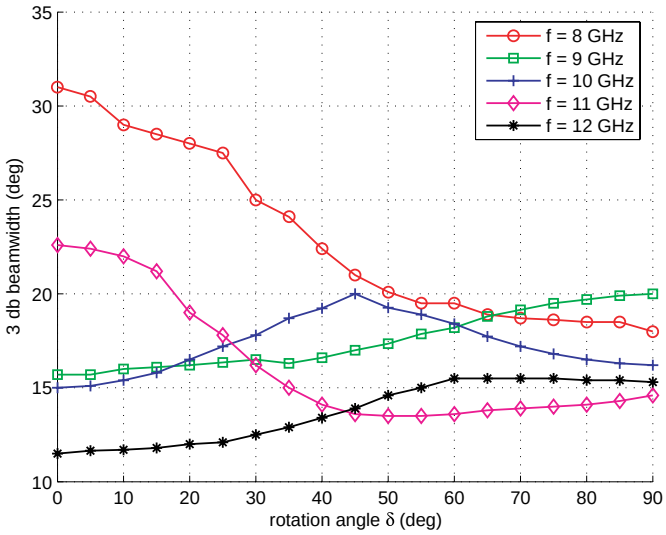

(b)

Figure 5. Variation of far field radiation quantities as function of the rotation angle δ of the elliptical scatterer with semi axes $a = 2\,\text{cm}$ and $b = 1\,\text{cm}$ for various operating frequencies f. Other parameters: $\epsilon_1 = 0.01$, $\mu_1 = 0.01$, $I = 1\,\text{A}$, $D = 8\,\text{cm}$, $d = 4\,\text{cm}$, $t = 6\,\text{cm}$. (a) Maximum radiated power (W/m) at $\phi = \pi/2$. (b) Three db beamwidth (degrees) from both sides of $\phi = \pi/2$.

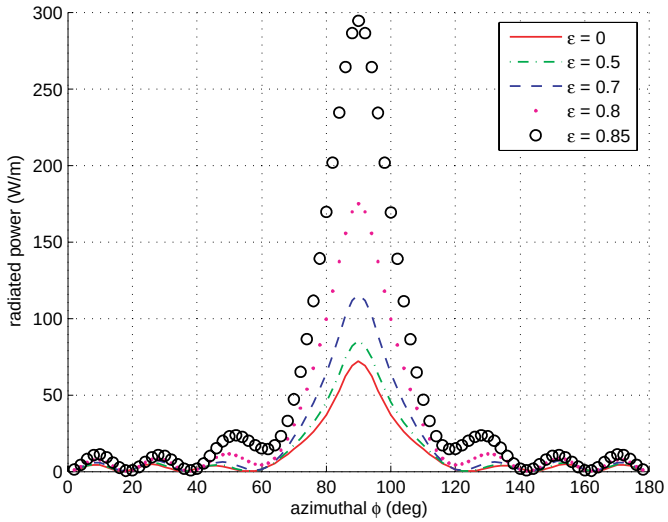

(a)

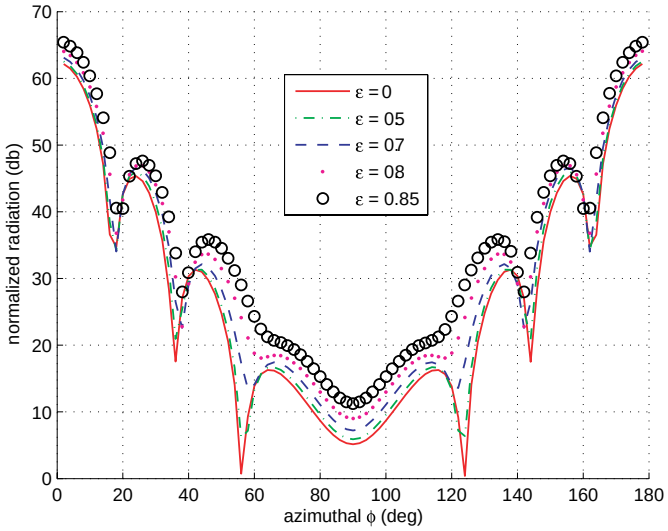

(b)

Figure 6. Variation of far field radiation quantities as function of the azimuthal ϕ for various eccentricities ϵ of the elliptical scatterer with semiminor axis $b = 1.5\,\text{cm}$. Other parameters: $\epsilon_1 = 0.01$, $\mu_1 = 0.01$, $I = 1\,\text{A}$, $f = 10\,\text{GHz}$, $D = 8\,\text{cm}$, $d = 4\,\text{cm}$, $t = 6\,\text{cm}$. (a) Radiated power (W/m) (b) Radiated power normalized by the corresponding power in the absence of the rod (db).

quantity is increasing as ϵ increases. As this happens for each azimuthal angle, large ϵ does not improve the features of the antenna.

The influence of the same elliptical scatterer on the functionality of the device was investigated with varying frequency. In Fig. 7a we present the variation of the maximum radiated power (at $\phi = \pi/2$) as function of the eccentricity of the ellipse. In these diagrams the interval of parameter ϵ is not equally divided because the shape of the scatterer is not significantly affected by variations of small ϵ and is substantially changed for large ones close to unity. For $f = 8$ and 9 GHz a remarkable stability is recorded while for greater frequencies alterations happen. Especially for $f = 10$ GHz a rapid increase on the radiated power is observed for $\epsilon > 0.5$. In Fig. 7b the represented quantity is the 3 db beamwidth. It is clear that for increasing frequency the angle is decreasing, making the antenna more directive. In this case the electrically larger scatterer improves the antenna.

The effect of the substrate's thickness on the characteristic quantities of the device is now investigated. In the example the source is located at $t = 7$ cm and four different cases of the substrate thickness are regarded: $d = 6, 5, 4$, and 3 cm with $D = 8$ cm. The scatterer is of constant curvature with $a = 1.5$ cm and the operating frequency is fixed at $f = 10$ GHz. In Fig. 8a we observe the variation of the radiated power of the total field as function of the angle ϕ. When d is large the radiated power is high but within a broad angular extent which means poor directivity. When d is small the radiated power is concentrated in the region of $\phi = \pi/2$ but the magnitude is reduced. The most satisfactory result is achieved for $d = 4$ cm, namely for a moderate substrate thickness, not too close to the scatterer. In Fig. 8b the polar plots of the surface current on the cylindrical scatterer are shown for the aforementioned cases. It is notable that the current on the bottom half of the scatterer is negligible. In these applications the cylinder is behaving as another antenna with maximum surface current at $\phi = \pi/2$.

The position of the source is another parameter of the problem the variation of which affects the operation of the device. Now d is constant equalling to 3 cm. Five cases of different t are observed: $t = 3.5, 4.5, 5.5, 6.5, 7.5$ cm. In Fig. 9a the radiated power becomes greater with decreasing t. The same happens for the surface electric current in Fig. 9b. These results are natural because if the source is located close to the PEC plane at $D = 8$ cm its presence is neutralized by the opposite image. The farther the electrical current it gets from the backing plane, the more powerful excitation exercises on the configuration.

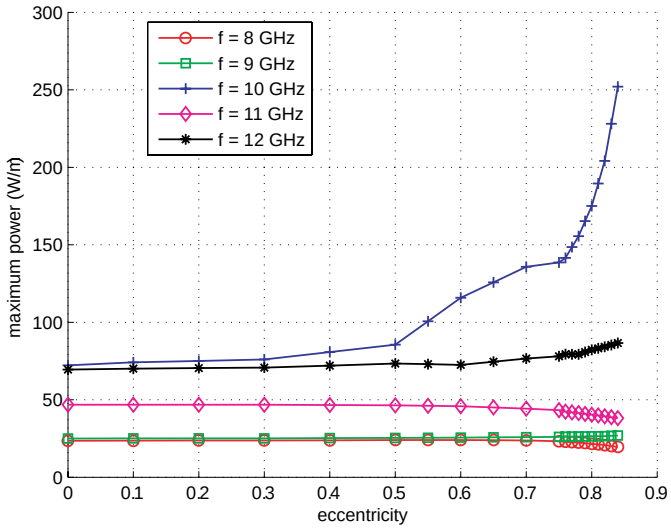

(a)

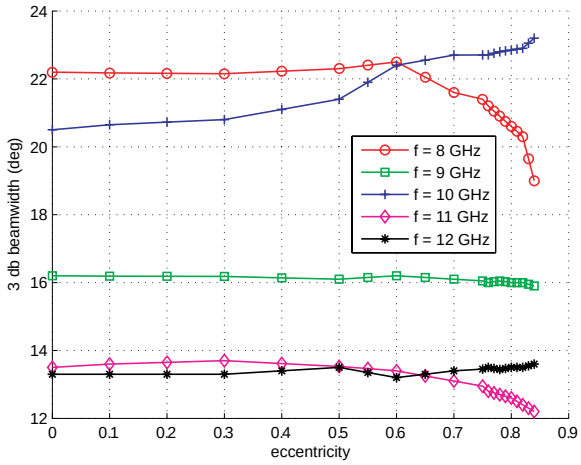

(b)

Figure 7. Variation of far field radiation quantities as function of the eccentricity ϵ of the elliptical scatterer with semiminor axis b =1.5 cm for various operating frequencies f. Other parameters: $\epsilon_1 = 0.01$, $\mu_1 = 0.01$, $I = 1\,\mathrm{A}$, $D = 8\,\mathrm{cm}$, $d = 4\,\mathrm{cm}$, $t = 6\,\mathrm{cm}$. (a) Maximum radiated power (W/m) at $\phi = \pi/2$. (b) Three db beamwidth (degrees) from both sides of $\phi = \pi/2$.

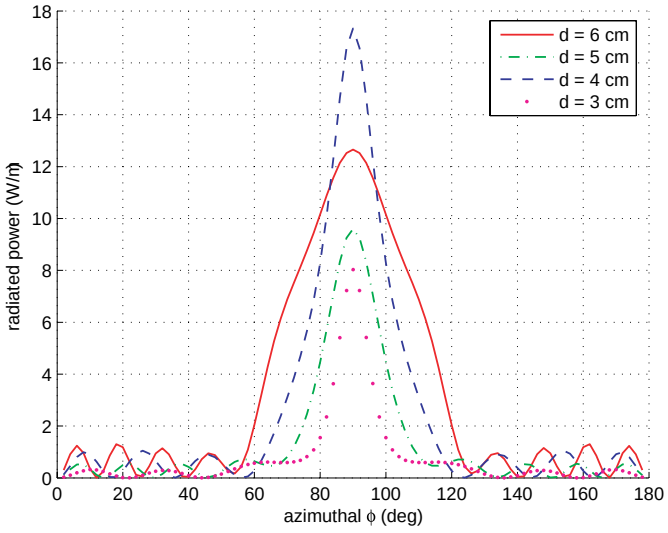

(a)

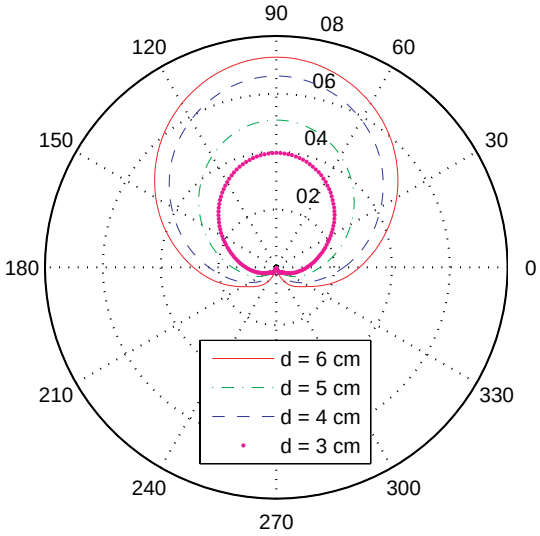

(b)

Figure 8. Variation of antenna quantities as function of the azimuthal ϕ for various substrate thicknesses $(D-d)$. The rod is circular with radius $a = 1.5\,\text{cm}$. Other parameters: ϵ_1 =0.01, μ_1 =0.01, $I = 1\text{A}$, $f = 10\,\text{GHz}$, $D = 8\,\text{cm}$, $t = 7\,\text{cm}$. (a) Radiated power (W/m) (b) Surface current (A/m) in polar plot.

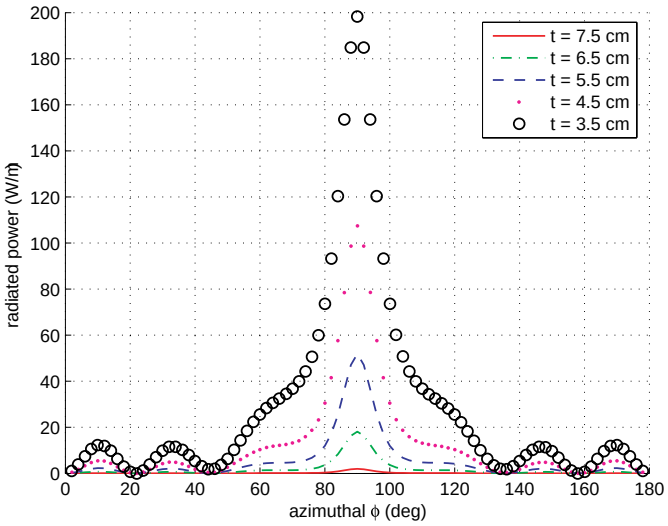

(a)

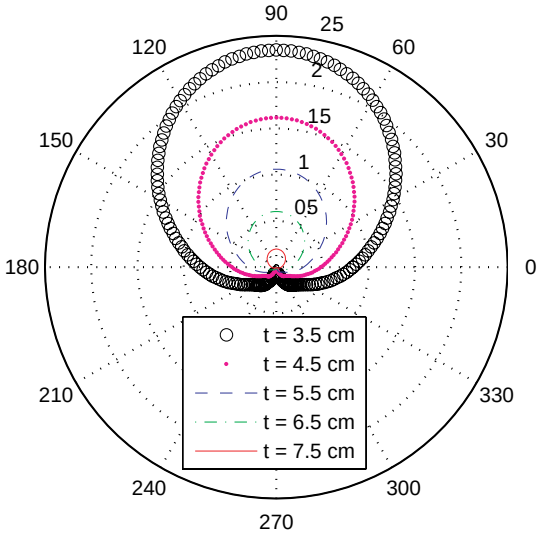

(b)

Figure 9. Variation of antenna quantities as function of the azimuthal ϕ for various substrate thicknesses t. The rod is circular with radius $a = 1.5\,\text{cm}$. Other parameters: $\epsilon_1 = 0.01$, $\mu_1 = 0.01$, $I = 1\,\text{A}$, $f = 10\,\text{GHz}$, $D = 8\,\text{cm}$, $d = 3\,\text{cm}$. (a) Radiated power (W/m) (b) Surface current (A/m) in polar plot.

7. CONCLUSION

The scattering of the field developed due to a metamaterial slab antenna by a PEC cylindrical scatterer located close to it is examined in the present work. The antenna is excited by a two–dimensional dipole inside the slab. In the mathematical formulation both method of auxiliary sources and method of moments are utilized. The case of rotated elliptical scatterer is examined and the variation of the antenna quantities as function of the rotation angle is observed. Also elliptical scatterers with arbitrary eccentricities are considered. Finally various substrate thicknesses and various source positions are investigated.

Several conclusions are drawn (some of them were expected by physical intuition) possibly useful for practical applications. They can also be compared with the corresponding ones emanating from the study of other similar problems such as the cases of dielectric or multilayered scatterer and the cases of multiple scatterers or multiple sources.

REFERENCES

1. Antoniades, M. and G. Eleftheriades, "A broadband Wilkinson balun using microstrip metamaterial lines," *IEEE Antennas Wireless Propag. Lett.*, Vol. 4, 209–212, 2005.
2. Mahmoud, S., "A new miniaturized annular ring patch resonator partially loaded by a metamaterial ring with negative permeability and permittivity," *IEEE Antennas Wireless Propag. Lett.*, Vol. 3, No. 10, 19–22, 2004.
3. Alu, A. and N. Engheta, "Achieving transparency with plasmonic and metamaterial coatings," *Phys. Rev. E*, Vol. 72, 016623, 2005.
4. Baccarelli, P., P. Burghignoli, G. Lovat, and S. Paulotto, "Surface–wave suppression in a double-negative metamaterial grounded slab," *IEEE Antennas Wireless Propag. Lett.*, Vol. 2, 269–272, 2003.
5. Baccarelli, P., P. Burghignoli, F. Frezza, A. Galli, P. Lampariello, G. Lovat, and S. Paulotto, "Fundamental modal properties of surface waves on metamaterial grounded slabs," *IEEE Trans. Microw. Theory Tech.*, Vol. 53, No. 4, 1431–1442, 2005.
6. Li, C., Q. Sui, and F. Li, "Complex guided wave solution of grounded dielectric slab made of metamaterials," *Progress In Electromagnetics Research*, PIER 66, 239–251, 2006.
7. Ubeda, E., J. Rius, and J. Romeu, "Preconditioning techniques in

the analysis of finite metamaterial slabs," *IEEE Trans. Antennas Propag.*, Vol. 54, No. 1, 265–268, 2006.

8. Parazzoli, C. G., R. B. Greegor, K. Li, B. E. C. Koltenbah, and M. Tanielian, "Experimental verification and simulation of negative index of refraction using Snell's law," *Phys. Rev. Lett.*, Vol. 90, 107401, 2003.
9. Lovat, G., P. Burghignoli, F. Capolino, D. Jackson, and D. Wilton, "Analysis of directive radiation from a line source in a metamaterial slab with low permittivity," *IEEE Trans. Antennas Propag.*, Vol. 54, No. 3, 1017–1030, 2006.
10. Wu, B., W. Wang, J. Pacheco, X. Chen, T. Grzegorczyk, and J. A. Kong, "A study of using metamaterials as antenna substrate to enhance gain," *Progress In Electromagnetics Research*, PIER 51, 295–328, 2005.
11. Pacheco, J., "Theory and application of left–handed metamaterials," 181–216, Ph.D. Dissertation, MIT, Cambridge, MA, 2004.
12. Wang, W., "Directive antenna using metamaterial substrates," 17–36, Master Thesis, MIT, Cambridge, MA, 2004.
13. Weng, Z.-B., Y.-C. Jiao, and F.-S. Zhang, "Design and experiment of one dimension and two dimension metamaterial structures for directive emission," *Progress In Electromagnetics Research*, PIER 70, 199–209, 2007.
14. Zitron, N. and J. Davis, "Scattering of directed radiation by a cylinder," *Journal Applied Scientific Research*, Vol. 18, No. 1, 280–287, 1968.
15. Felsen, L. and N. Marcuvitz, *Radiation and Scattering of Waves* , 485–487, Wiley-IEEE, New York, 1994.
16. Valagiannopoulos, C. A., "Arbitrary currents on circular cylinder with inhomogeneous cladding and RCS optimization," *Journal of Electromagnetic Waves and Applications*, Vol. 21, No. 5, 665–680, 2007 (scheduled for publication).
17. Pinto, I., V. Galdi, and L. Felsen, *Electromagnetics in a Complex World: Challenges and Perspectives*, 155–157, Springer, Benevento, 2004.
18. Schevchenko, V., *Continuous Transitions in Open Waveguides*, 24–26, Golem, 1971.
19. Leviatan, Y. and A. Boag, "Analysis of electromagnetic scattering from dielectric cylinders using a multifilament current model," *IEEE Trans. Antennas Propag.*, Vol. 35, No. 10, 1119–1128, 1987.
20. Leviatan, Y., P. Li, A. Adams, and J. Perini, "Single-post inductive obstacle in rectangular waveguide," *IEEE Trans.*

Microw. Theory Tech., Vol. 31, No. 10, 806–812, 1983.

21. Leviatan, Y. and A. Boag, "Analysis of electromagnetic scattering from dielectrically coated conducting cylinders using a multifilament current model," *IEEE Trans. Antennas Propagat.*, Vol. 36, No. 11, 1602–1607, 1988.
22. Karkashadze, D., "On Status of main singularities in 3D scattering problems," *Proceedings of VIth International Seminar/Workshop on DIPED-2001*, 81–84, 2001.
23. Stewart, J., *Calculus*, 575–581, Brooks/Cole Publishing Company, 1999.
24. Fikioris, G., "On two types of convergence in the method of auxiliary sources," *IEEE Trans. Antennas Propagat.*, Vol. 54, No. 7, 2022–2033, 2006.
25. Erdelyi, A., *Asymptotic Expansions*, 50–52, Dover Publications, New York, 1956.
26. Li, L., D. You, M. Leong, and T. Yeo, "Electromagnetic scattering by multilayered chiral-media structures: a scattering radiation transform," *Progress In Electromagnetic Research*, PIER 26, 249–291, 2000.
27. Abramowitz, M. and I. Stegun, *Handbook of Mathematical Functions*, 362–364, National Bureau of Standards, Washington, 1964.
28. Hildebrand, F., *Advanced Calculus for Applications*, 549–551 Prentice Hall, New Jersey, 1976.
29. Jones, D., *Theory of Electromagnetism*, 269–271, Pergamon Press, Oxford, 1964.
30. Collin, R., *Field Theory of Guided Waves*, 730–732, IEEE Press, New York, 1991.